HHS Public Access

Author manuscript

Cell Rep. Author manuscript; available in PMC 2021 March 09.

Published in final edited form as:

Cell Rep. 2021 January 26; 34(4): 108669. doi:10.1016/j.celrep.2020.108669.

DCAF14 promotes stalled fork stability to maintain genome integrity

Arik Townsend[1,2], **Gabriella Lora**[1,2], **Justin Engel**[1,2], **Neysha Tirado-Class**[1], **Huzefa Dungrawala**[1,3,*]

[1]Department of Cell Biology, Microbiology and Molecular Biology, University of South Florida, Tampa, FL 33620, USA

[2]These authors contributed equally

[3]Lead contact

SUMMARY

Replication stress response ensures impediments to DNA replication do not compromise replication fork stability and genome integrity. In a process termed replication fork protection, newly synthesized DNA at stalled replication forks is stabilized and protected from nuclease-mediated degradation. We report the identification of DDB1- and CUL4-associated factor 14 (DCAF14), a substrate receptor for Cullin4-RING E3 ligase (CRL4) complex, integral in stabilizing stalled replication forks. DCAF14 localizes rapidly to stalled forks and promotes genome integrity by preventing fork collapse into double-strand breaks (DSBs). Importantly, $CRL4^{DCAF14}$ mediates stalled fork protection in a RAD51-dependent manner to protect nascent DNA from MRE11 and DNA2 nucleases. Thus, our study shows replication stress response functions of DCAF14 in genome maintenance.

In Brief

Townsend et al. find that DDB1- and CUL4-associated factor DCAF14 is recruited to stalled replication forks. DCAF14 prevents replication fork collapse in a CRL4-dependent manner to promote genome stability and cell survival. DCAF14 depletion triggers nascent strand degradation that is reversible by enhancing RAD51 levels at forks.

Graphical Abstract

*Correspondence: hdungrawala@usf.edu.

AUTHOR CONTRIBUTIONS

A.T., G.L., and J.E., under supervision of H.D., and H.D. performed the experiments. N.T.-C. performed the immunoprecipitation (IP) assay. H.D. conceived the project, designed the study, and wrote the manuscript. All authors edited the manuscript.

SUPPLEMENTAL INFORMATION

Supplemental Information can be found online at https://doi.org/10.1016/j.celrep.2020.108669.

DECLARATION OF INTERESTS

The authors declare no competing interests.

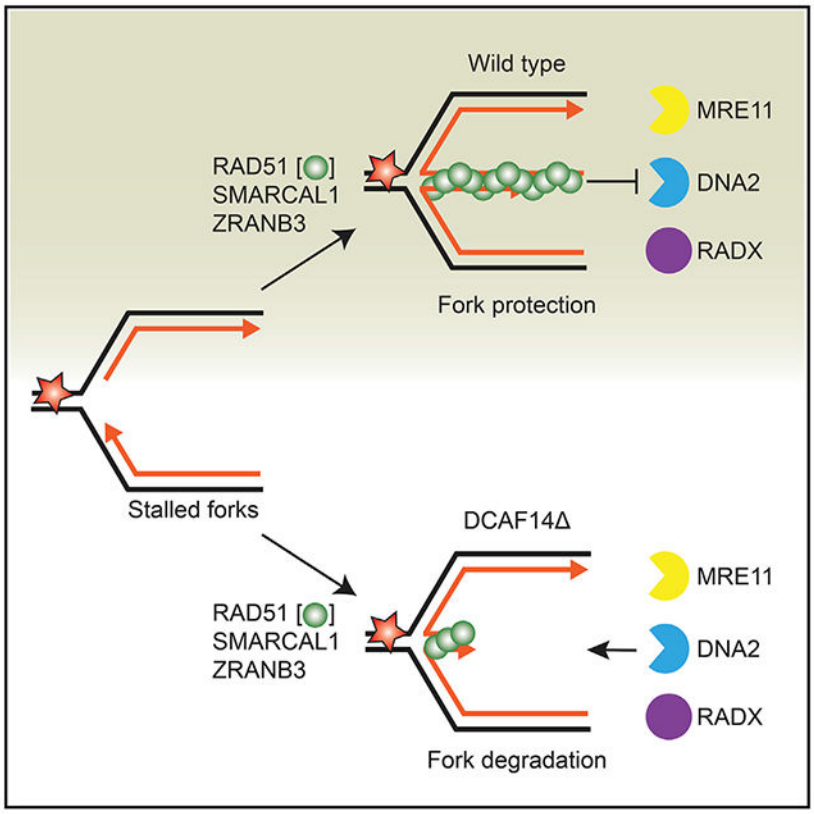

INTRODUCTION

Cells must duplicate their genome accurately and completely during each cell division cycle. Replication is inherently challenged by various exogenous and endogenous stresses that act as obstacles stalling active replication forks. Failure to deal with replication stress compromises fork stability and genome integrity, resulting in increased predisposition to diseases such as cancer.

Stalled forks recruit multiple stress response proteins to promote stability, repair, and restart of damaged forks, thereby preventing spontaneous collapse into double-strand breaks (DSBs) (Cimprich and Cortez, 2008; Saldivar et al., 2017). Homologous recombination (HR) repair proteins BRCA1/2 and Fanconi anemia (FA) are increasingly being recognized for critical functions in remodeling and protecting stalled replication forks to preserve genome integrity (Kolinjivadi et al., 2017a; Datta and Brosh, 2019). Importantly, determinants of replication fork protection modulate response to chemotherapy, highlighting the clinical relevance of this process in cancer therapy (Sidorova, 2017; Liao et al., 2018).

A universal response to genotoxic stress is replication fork reversal (or fork regression), a genome maintenance mechanism that converts three-way junctions to four-way junctions, resulting in reannealing of nascent DNA strands behind the fork (Higgins et al., 1976; Neelsen and Lopes, 2015). Various motor proteins such as SMARCAL1 (Bétous et al., 2012), ZRANB3 (Ciccia et al., 2012), and HLTF (Kile et al., 2015) catalyze fork reversal. In

a manner distinct from DSB repair, HR pathway proteins stabilize and protect the regressed arm of reversed replication forks from MRE11-dependent degradation (Schlacher et al., 2011,2012; Mijic et al., 2017; Kolinjivadi et al., 2017b). Other genetic perturbations cause DNA2-dependent nascent DNA digestion (Wang et al., 2015; Xu et al., 2017; Higgs et al., 2015). Central to fork protection is the ability of BRCA2 to generate stable RAD51 nucleoprotein filaments on the regressed arm of reversed replication forks. RAD51 is also essential to promote replication fork reversal (Zellweger et al., 2015). As such, suppressing fork reversal or nuclease activities restores replication fork protection (Taglialatela et al., 2017; Mijic et al., 2017; Ray Chaudhuri et al., 2016). Stalled fork protection is also dictated by proteins altering the stability of chromatin-bound RAD51. While BOD1L loss (Higgs et al., 2015) triggers nascent strand degradation, suppressing RADX can reverse nascent strand degradation and chemosensitivity by increasing RAD51 association with stalled forks (Dungrawala et al., 2017).

Cullin4-RING E3 ubiquitin ligases (CRL4s) are multi-subunit protein complexes that ubiquitinate target proteins to regulate a diverse range of cellular processes (Jackson and Xiong, 2009). CRL4s utilize DDB1- and CUL4-associated factors (DCAFs) as substrate receptors to recruit substrates for ubiquitination. DCAF14 (or PHIP, RepID) is one of 18 known CRL4 substrate receptors (Jin et al., 2006). Human DCAF14 functions in mitogenesis (Farhang-Fallah et al., 2002; Podcheko et al., 2007), replication origin initiation (Zhang et al., 2016), and regulation of the spindle assembly checkpoint (Jang et al., 2020). DCAF14 is also a prognostic biomarker for metastatic melanoma (De Semir et al., 2012), and deleterious *de novo* mutations in DCAF14 are associated with developmental abnormalities (Webster et al., 2016; Craddock et al., 2019). However, it is not known whether DCAF14 functions in conditions of perturbed replication.

Herein, we report a previously uncharacterized function of DCAF14 in replication stress response. When replication is challenged, DCAF14 is recruited to stalled forks and protects nascent DNA from nuclease-mediated digestion in a CRL4-dependent manner, thus preventing fork collapse into toxic DSBs. In cells devoid of DCAF14, fork degradation can be reversed by restoring RAD51's ability to form stable nucleoprotein filaments. Thus, $CRL4^{DCAF14}$ plays a critical role in promoting stalled fork stability and genome integrity.

RESULTS

DCAF14 is enriched at stalled replication forks

Replication fork proteomic screens using iPOND (isolation of proteins on nascent DNA) coupled with SILAC (stable isotope labeling of amino acids in cell culture) mass spectrometry were performed previously to study protein dynamics in response to replication stress (Dungrawala et al., 2015). In these studies, fork proteomes of untreated cells were compared with cells exposed to hydroxyurea (HU) for 5 min up to 240 min (Figure 1A). Histone accumulation remains unchanged throughout the HU time course (Dungrawala et al., 2015). While the CMG helicase components MCM2-7 decrease in abundance due to slowed termination events, replication stress response proteins such as single-stranded DNA (ssDNA) binding protein RPA increase in abundance (Figure 1B). Like RPA, DCAF14 is rapidly recruited and persists up to 4 h of HU treatment (Figure 1B). Using

proximity ligation assay, we observe significantly elevated levels of DCAF14/RPA foci in cells exposed to replication stress (Figure 1C). These results indicate that DCAF14 is recruited to stalled replication forks.

DCAF14 functions as a replication stress response protein

We performed loss-of-function studies to investigate whether DCAF14 functions in replication stress response. Transient depletion of DCAF14 using small interfering RNA (siRNA) increases S-phase-associated γH2AX levels in untreated U2OS cells (Figures 2A and 2B). By comparison, exposure to replication stress markedly escalates γH2AX, indicating that loss of DCAF14 exacerbates replication stress. This phenotype is not due to off-target effects since multiple siRNAs targeting DCAF14 (Figures S1A and S1C) and two independent DCAF14 knockout (KO) clones (Figures S1B and S1D) yield similar responses to HU. The replication-stress-associated γH2AX increase in DCAF14-deficient cells occurs concomitantly with increased ssDNA, as examined by staining for bromo-deoxyuridine (BrdU)-labeled DNA in non-denaturing conditions (Figure 2C) and detergent-resistant RPA (Figure 2D). DCAF14-depleted cells also exhibit sensitivity to multiple replication-stress-inducing reagents including HU, camptothecin (CPT), olaparib, and cisplatin (Figures 2E and S1E). Cell-cycle analyses revealed no observable changes in S-phase distribution using both siDCAF14 and DCAF14 KO cells (Figures S1F). Consistent with heightened genome instability and drug sensitivity, DCAF14-deficient cells display increased G1-phase-specific 53BP1 bodies (Figure 2F), indicating that unresolved replication stress persists through mitosis. Thus, DCAF14 absence results in failure to deal with replication stress.

Direct repeat (DR)-GFP reporter U2OS cells were utilized to assess whether DCAF14 is required for HR-mediated break repair. While silencing BRCA2 abrogates HR, DCAF14-deficient cells exhibit a modest defect in HR efficiency (Figure 2G). Infrared (IR)-induced sensitivity (Figures S1G) and break recovery (Figures S1H) also remain unaltered in DCAF14-deficient cells, indicating that DCAF14 does not regulate break repair.

DCAF14 stabilizes stalled replication forks

To gain mechanistic insight into DCAF14 function at stalled replication forks, we examined single replicating molecules of DNA using fiber-labeling analyses (Figure 3A). While elongation rates remain unchanged with DCAF14 deficiency in unchallenged cells (0.33 versus 0.32 μm/min), fiber lengths are significantly shortened with CPT treatment in DCAF14-deficient cells (Figure 3B), resulting in reduced IdU/CldU ratios (Figure 3C). Similar defects also occurred in RPE-hTERT cells and HEK293T cells (Figure S2A) and can be rescued by complementing DCAF14 KO cells with DCAF14 cDNA (Figure 3D). We also observed a marginal increase in origin firing when replication is challenged in DCAF14-deficient cells (Figure S2B). Thus, DCAF14 loss curtails DNA replication in perturbed conditions.

Next, we immunoprecipitated FLAG-tagged DCAF14 from HU-treated cells and validated the association with CRL4 components (Figure 3E). We then asked whether depleting DDB1 and CUL4 paralogs CUL4A and CUL4B phenocopy fork elongation defects observed in DCAF14-deficient cells. While silencing DDB1 and CUL4B limits fork

elongation in CPT, CUL4A depletion using multiple siRNAs has no effect (Figures 3F and Figure S2C). These data are consistent with continued association of DDB1 and CUL4B at replication forks after HU-induced fork stalling in previous iPOND proteomic screens (Figure S2D). During the course of our immunoblotting analyses, we observed CUL4A depletion causes a marked increase in the slower migrating form of CUL4B, which represents neddylated species (Figure 3G). The E3 activity of CRLs is triggered by a 9-kDa covalent addition of NEDD8 (Pan et al., 2004), and our data suggest that CUL4B exists in predominantly neddylated state when CUL4A is absent. By contrast, CUL4A migration pattern after CUL4B depletion remains unchanged, suggesting that CUL4A is dispensable for CRL4 activity when fork stalling occurs. The elongation defect in DCAF14-deficient cells is also not additive with co-depletion of either DDB1 or CUL4B (Figure S2E), further indicating that $CRL4^{DCAF14}$ promotes stalled fork stability.

Defective fork progression is indicative of unscheduled fork collapse into DSBs (Cortez, 2015). DNA fiber analyses reveal that fork recovery is diminished in DCAF14-deficient cells compared with control cells (Figures 3H and S2F). Indeed, cells devoid of DCAF14 also display increased breaks after HU treatment as assessed by neutral comet assay (Figures 3I and S2G). Collectively, these results demonstrate that DCAF14 stabilizes stalled replication forks to prevent irreversible collapse into DSBs.

DCAF14 prevents nascent strand degradation

Given that DCAF14 stabilizes stalled forks, we sought to investigate whether newly synthesized DNA is prone to any processing events in the context of DCAF14 deficiency. For this purpose, we utilized a DNA fiber-labeling approach previously described (Schlacher et al., 2011) to monitor the stability of nascent DNA (Figure 4A). Upon HU exposure, we observe fork degradation in siDCAF14-transfected cells and three independent DCAF14 KO clones (Figures 4B and S4A). Silencing DDB1 and CUL4B also yields similar fork degradation phenotypes (Figure S3A), indicating that $CRL4^{DCAF14}$ promotes stalled fork protection.

To determine the nuclease responsible for fork degradation, we silenced MRE11 and DNA2 in DCAF14-deficient cells. Eliminating both MRE11 (Figures 4C and S4B) and DNA2 (Figures 4D and S4C) individually restores fork protection, indicating that DCAF14 loss facilitates both MRE11- and DNA2-dependent degradation. We also transiently depleted SMARCAL1 and ZRANB3 to ask whether fork remodeling is a prerequisite for nascent DNA digestion in DCAF14-depleted cells. Codepleting SMARCAL1 or ZRANB3 is sufficient to reverse fork degradation (Figures 4E and S4D), consistent with a previous report highlighting cooperative function of fork remodelers in promoting fork degradation (Taglialatela et al., 2017). SMARCAL1 or ZRANB3 co-depletion also restores fork protection in DDB1- and CUL4B-depleted cells (Figure S3B and S4E). Thus, SMARCAL1 and ZRANB3 remodel forks for DNA2- and MRE11-mediated nascent DNA digestion when DCAF14 is absent. Since DNA2-dependent hyper-resection drives fork degradation in BOD1L- and ABRO1-deficient cells, we probed for phosphorylated RPA S4/S8 levels to measure extent of resection. Whole-cell lysates and chromatin fractions isolated from HU-treated siDCAF14-transfected cells and DCAF14 KO cells, respectively, show minimal

changes in RPA S4/S8 levels by immunoblotting (Figure 4F), suggesting that DCAF14 does not function to block excessive resection.

BRCA2 stabilizes RAD51 nucleoprotein filaments to suppress nascent strand degradation. Thus, we co-depleted DCAF14 with either BRCA1 or BRCA2 to determine epistasis and observed that fork degradation phenotype was not additive (Figures 4G, S3C, S4F, and S4G). In response to replication stress, DCAF14-deficient cells are not defective in RAD51 foci formation (data not shown), which suggests DCAF14 functions downstream of BRCA2. Thus, we interrogated fork protection functions of RAD51 in the context of DCAF14 deficiency. We began by asking whether silencing RAD51 rescues fork degradation in DCAF14-depleted cells since RAD51 promotes fork reversal in BRCA2-deficient cells (Mijic et al., 2017). Consistent with previous observations (Bhat et al., 2018), silencing RAD51 using two potent siRNAs does not cause nascent strand degradation (Figures 4H and S4H). Under these circumstances, fork degradation is alleviated in DCAF14-deficient cells, suggesting that RAD51-mediated fork remodeling promotes nascent DNA digestion in cells lacking DCAF14. Since suppressing fork remodeling restores fork protection, we reasoned that RAD51-mediated filament stabilization is impaired when DCAF14 is absent. To test this hypothesis, DCAF14-deficient cells were transfected with constructs expressing wild-type (WT) RAD51 and ATPase-deficient RAD51 (K133R). K133R RAD51 is defective in ATP hydrolysis (Morrison et al., 1999) and forms hyperstable filaments (Sigurdsson et al., 2002). Overexpressing RAD51 or K133R RAD51 rescues fork degradation in FANCD2- and BRCA2-deficient cells (Schlacher et al., 2011, 2012). Consistent with our hypothesis, overexpressing both WT RAD51 and K133R RAD51 restores fork protection in DCAF14-deficient cells (Figures 4I and S4I). We also asked whether RADX removal reverses fork degradation since depleting RADX restores fork protection in cells devoid of BRCA, FANCA/D2, and BOD1L. Indeed, silencing RADX was sufficient to suppress fork degradation and chemosensitivity in DCAF14-deficient cells (Figures 4J, S3E, and S4J). Depleting anti-recombinase BLM also restores fork protection in DCAF14-deficient cells (Figure S3D). Overall, these data indicate that DCAF14 promotes replication fork protection in a RAD51-dependent manner.

DISCUSSION

Here, we report the replication stress response functions of $CRL4^{DCAF14}$ in facilitating stalled fork stability and genome integrity. Mechanistically, DCAF14 acts at stalled forks to protect newly synthesized DNA from nuclease-mediated degradation. We propose a model wherein DCAF14 regulates RAD51 filament formation on regressed arms of reversed replication forks. Consistent with this interpretation, overexpressing RAD51 or the ATPase-deficient K133R RAD51 mutant restores fork protection, as observed previously in BRCA2- and FANCD2-defective cells. Moreover, removal of RAD51 antagonist RADX or anti-recombinase BLM also suppresses fork degradation. Thus, restoring RAD51 nucleoprotein filament stability at forks is sufficient to impart replication fork stabilization when DCAF14 is absent. Our results also suggest that RAD51-mediated fork remodeling persists in DCAF14-deficient cells since depleting RAD51, SMARCAL1, and ZRANB3 reverse fork degradation, supporting the model that fork remodeling provides substrates for nuclease-mediated degradation. We speculate that fork degradation occurs at reversed replication

forks in DCAF14-deficient cells, as observed in cells with compromised BRCA2 function (Mijic et al., 2017; Taglialatela et al., 2017; Kolinjivadi et al., 2017b).

We also find that DCAF14 suppresses fork degradation from MRE11 and DNA2 nucleases. A possible explanation is that both nucleases cooperate in processing DNA at similar replication intermediates. Alternatively, the nucleases could be acting on different replication intermediates during fork remodeling events. Nevertheless, the dependency on MRE11 and DNA2 is consistent with our model that RAD51 regulates fork protection in DCAF14-deficient cells since defective RAD51 stabilization induces MRE11-dependent degradation in BRCA2-deficient cells (Schlacher et al., 2011) and DNA2-dependent degradation in BOD1L-deficient cells (Higgs et al., 2015). Consistent with these interpretations, RADX silencing also restores fork protection since loss of RADX protects forks from MRE11 and DNA2 nucleases (Bhat et al., 2018; Dungrawala et al., 2017). Although RADX depletion suppresses replication-stress-induced chemosensitivity in DCAF14-deficient cells, further studies are necessary to establish whether fork protection modulates chemosensitivity across multiple genetic contexts.

Our results further demonstrate that the absence of CRL4 components DDB1 and CUL4B phenocopy DCAF14, consistent with the notion that $CRL4^{DCAF14}$ modulates replication fork stability in response to replication stress. Interestingly, silencing CUL4A does not alter fork elongation in CPT, indicating that CUL4A is non-essential for stabilizing stalled replication forks. Although CUL4A and CUL4B perform overlapping roles, distinct functions have been previously reported for both CUL4 family members. While lesion recognition is primarily mediated by $CRL4A^{DDB2}$, CUL4B mutations are associated with X-linked mental retardation (Liu et al., 2012). Whether $CRL4^{DCAF14}$ preferentially occupies CUL4B at perturbed forks is not known. Additionally, further studies are required to determine dependency on ubiquitin signaling for $CRL4^{DCAF14}$ function at stalled forks and whether the complex modulates RAD51 activity directly or indirectly through other RAD51 regulators. Altogether, our study identifies DCAF14 as a fork protection component that functions to mitigate replication stress and provides a potential avenue to exploit CRL4 function to target fork vulnerabilities for chemotherapy.

STAR ★METHODS

RESOURCE AVAILABILITY

Lead contact—Further information and requests for resources and reagents should be directed to and will be fulfilled by the Lead Contact, Huzefa Dungrawala (hdungrawala@usf.edu).

Materials availability—Cell lines generated in this study are available upon request from the lead contact.

Data and code availability—Original data for immunoblots in the paper are available (http://dx.doi.org/10.17632/2785zxsyzd.1)

EXPERIMENTAL MODEL AND SUBJECT DETAILS

U2OS, HEK293T and DR-GFP U2OS reporter cell lines were cultured in DMEM with 7.5% FBS and 5% CO2 while RPE-hTERT were grown in DMEMF12 with 7.5% FBS and 7.5% NaHCO3. All cells were incubated at 37C with 5% CO2. U2OS and RPE-hTERT are female.

METHOD DETAILS

Generation of DCAF14 knockout (KO) cell lines—U2OS and HEK293T DCAF14 KO cell lines were generated using CRISPR/Cas9. Briefly, cells were co-transfected with pSpCas9 (BB)-2A-Puro vectors carrying guide RNAs targeting exon1-intron1 junction (GCTGCGATCGGGTAAGTCGG) and exon4 (GCGCACCGACTGGACCGGGA). Two days post puromycin selection, single cells were seeded using 96-well dishes. Single cell colonies were isolated after 2-3 weeks and screened for DCAF14 gene editing using PCR and immunoblotting.

Transfections—Plasmid transfections were carried out using FUGENE HD (Promega) in U2OS cells and polyethylenimine in HEK293T cells. siRNA transfections in U2OS cells were performed using Dharmafect1 (Dharmacon). All assays were performed 3 days post transfection for siRNA transfected samples and 4 days post transfection for plasmid transfected samples.

Antibodies, siRNAs and plasmids—The following antibodies were used for immunofluorescence (IF) and western blotting (WB) where indicated: anti-phospho-histone H2AX clone JBW301 (1:9000, IF, 05-636, Millipore), 53BP1 (1:300, IF, ab21083, Abcam), PCNA PC10 (1:300, IF, sc-56, SantaCruz), CHK1 G-4 (1:1000, WB, sc-8408, SantaCruz), SMARCAL1 (1:1000, WB, sc-376377, SantaCruz), ZRANB3 (1:1000, WB, A303-033A, Bethyl), BRCA1 (1:100, WB, sc-6954, Santa Cruz), BRCA2 (1:250, WB, OP95, Millipore), KU70 (1:2000, WB, ab92450, Abcam), RAD51 (1:1000, WB, ab63801, Abcam), Histone H3 (1:10,000, WB, ab1791, Abcam), RPA32 9H8 (1:1000, WB, ab2175, Abcam), Phospho RPA32 S4S8 (1:1000, WB, A300-245A, Bethyl), DCAF14/PHIP (1:500, WB, NBP2-33883, Novus and 1:200, IF, ab86244, Abcam), BLM (1:1000, WB, sc-365753, SantaCruz), MRE11 (1:1000, WB, 4895S, Cell Signaling), RADX (1:1000, WB, NBP2-13887, Novus), DNA2 (1:250, WB, PA5-77943, Invitrogen), CUL4A (1:500, WB, ab72548, Abcam), CUL4B (1:500, WB, VMA00360, Bio-rad) and DDB1 (1:1000, WB, 5428S, Cell Signaling Tech). Mouse anti-BrdU (1:100, 347580, BD) and rat anti-BrdU (1:100, ab6326, Abcam) were used for DNA fiber analyses to recognize IdU and CldU respectively. For proximity ligation analyses, mouse anti-RPA (1:200) and rabbit anti-DCAF14 (1:500) were utilized. ON-TARGETplus siRNAs were purchased from Dharmacon for all transient knockdown experiments except where specified. Four different siRNAs targeting the open reading frame of DCAF14 were purchased for knockdown validation: J-019291-05 (CAACACAAUUAUCGUACAA), J-019291-06 (UAAACUGACUGGCGGAUCA), J-019291-07 (GCACGUAUUUGGCAAUUUA) and J-019291-08 (GAUGGGAGGUUGUUAGCUA). J-019291-06 siRNA was used for all DCAF14 knockdown experiments. Other siRNAs used in this study: DDB1 (L-012890), RADX (J-014634), RAD51 (J-003530-11), RAD51 (J-003530-12), MRE11 (J-009271-08), BLM

(L-007287), SMARCAL1 (J-013058-06), CUL4A (L-012610), CUL4B (L-017965), DNA2 (pool of D-026431-03 and D-026431-04, siGENOME Dharmacon), ZRANB3 (D-010025-03, siGENOME Dharmacon), BRCA1 (J-003461), BRCA2-6 (SI02653434, QIAGEN) and All-stars negative control siRNA (1027280, QIAGEN). DCAF14 cDNA clone (RC217114) and the entry vector (PS100001) were purchased from Origene. Human RAD51 (Item ID = 125570) and RAD51K133R (Item ID = 125571) expressing vectors were purchased from Addgene. All vectors were validated by sequencing.

Viability assays—For long-term survival assays, U2OS cells transfected with either non-targeting siRNA or DCAF14 siRNA were seeded in 60mm dishes for single colonies in triplicates. Cells were treated with HU and CPT for 24 hours and released into fresh media the following day whereas olaparib and cisplatin were left in the media for the duration of the assay. Colonies were fixed, stained and quantified after approximately 3-4 weeks using methylene blue (48% methanol, 2% methylene blue and 50% water). Plating efficiencies and survival fractions were calculated as described previously (Franken et al., 2006). Survival measurements were calculated as percentage of untreated control. All clonogenic survival assays were completed using three repeats.

Flow cytometry—For cell cycle analyses, cells were harvested following trypsinization, fixed in 70% ethanol, and treated with propidium iodide and RNase. To measure HR efficiency using GFP reporter cells, DR-GFP U2OS cells were transfected with the respective siRNAs in a 6-well dish. After refreshing the media next day, cells were transfected using 2ug of I-SceI expressing plasmid pCBASecI to induce DSBs. Post 72 hours, cells were harvested and analyzed immediately using flow cytometry. All flow cytometry analyses were carried out on BD FACSCanto II.

Immunofluorescence—For immunofluorescence analyses, detergent extraction was performed using 0.5% Triton X-100 prior to fixation using 3% paraformaldehyde/2% sucrose. For all experiments probing for DCAF14, cells were fixed with 4% paraformaldehyde. After blocking with 5% BSA/PBS, cells were incubated with primary and secondary antibodies and coverslips were mounted using Prolong Gold with DAPI (Invitrogen). To detect changes in exposed single-stranded DNA, cells were pulsed with 10uM BrdU for 10min. Where mentioned, cells were prelabeled using 10uM EdU for desired times to select cells in S-phase. Genome incorporated EdU was detected by click chemistry using Alexa Fluor 488 or 594 azide. Proximity ligation assays (PLA) were performed using Duolink *In Situ* Mouse/Rabbit Kit (Sigma) following manufacturer's instructions. Images were acquired on Keyence BZ-X710 All-in-one fluorescence microscope using 20X objective (0.75NA) and analyzed using Cell Profiler.

Immunoprecipitation—HEK293T cells were transfected with either empty vector or DCAF14-MYC-FLAG vector. After 4hr of HU treatment, lysates were extracted using extraction buffer (50mM Tris-Cl, 150mM NaCl, 1% Triton X-100, 1mM Aprotinin, 1mM Leupeptin, 10mM NaF and 10mM β-glycerol phosphate) in presence of nuclease. After preclearing for 1 hour, lysates were incubated with FLAG magnetic beads (Sigma) overnight. Beads were washed 3X with extraction buffer, once with TBS and captures were

eluted by boiling in sample buffer. The co-immunoprecipitates were separated by SDS-PAGE and proteins identified by immunoblotting.

Neutral Comet assay—DNA double strand breaks were detected using Trevigen comet assay kit. Tail moments were scored using Comet Score software (Tritek) and data presented as box and whisker plots.

DNA fiber analysis—DNA fiber labeling analysis was carried out essentially as described previously (Jackson and Pombo, 1998). For nascent strand degradation analysis, cells were sequentially pulsed with 20uM CldU and 100uM IdU for 30 min each followed by release into 4mM HU for 4 hours. To analyze fork elongation in presence of CPT, cells were pulsed with CldU for 30min, followed by IdU in presence of 100nM CPT for 30min. To assess fork recovery after release from replication stress, cells were pulsed with CldU for 30min, washed, released into 4mM HU for 4 hours, washed aging and pulsed with IdU for 60 min. Following treatments, cells were harvested, lysed on slides and DNA was stretched by tilting the slides. DNA was then fixed using 3:1 solution of methanol:acetic acid and stored at −20C overnight. Next day, DNA was denatured using 2.5N HCl for 70min, blocked in PBS containing 0.1% Triton X-100 and 10% goat serum, stained with primary antibodies for 2 hours to recognize IdU and CldU followed by staining with secondary antibodies for 1 hour. Images were acquired using a 60X oil objective (1.4NA) on Keyence BZ-X700 and fiber lengths were analyzed using ImageJ.

Whole cell lysate and chromatin extraction—Whole cell lysates were prepared by incubating cells on ice for 30 minutes in RIPA lysis buffer (50mM Tris-Cl pH = 7.4,1% NP-40, 150mM NaCl, 0.1% SDS, 1mM DTT, 0.5% Sodium deoxycholate, 1mM Aprotinin, 1mM Leupeptin, 1mM PMSF and 1mM Sodium Orthovanadate) supplemented with Pierce universal nuclease. Chromatin extractions were performed essentially as previously described (Méndez and Stillman, 2000).

QUANTIFICATION AND STATISTICAL ANALYSIS

All statistical analyses were completed using Graphpad Prism 8 (Graphpad). For pairwise comparisons of samples conforming to normal distribution, two-tailed t tests with Welch's correction or FDR-corrected multiple t tests were utilized. One-way ANOVA tests with Tukey's multiple comparisons were used for comparing three or more samples. For all other statistical analyses, two-tailed Mann-Whitney tests were utilized. All significance values were derived using p value = 0.05 as cutoff. Statistical details can be found in the figure legends including sample size, definition of center and dispersion measures, statistical test and significance values. No statistical methods were adopted for randomization, sample size estimation and inclusion/exclusion of data. All experiments were performed at least twice.

Supplementary Material

Refer to Web version on PubMed Central for supplementary material.

ACKNOWLEDGMENTS

We thank David Cortez and Kristina Schmidt for helpful discussions and valuable feedback. We thank USF COM Fred Wright Jr Flow Cytometry Core for flow cytometry analyses and Adam Weaver for providing access to X-ray system at Moffitt Cancer Center. We thank Jeremy Stark for providing DR-GFP U2OS reporter cells. CMV-hRad51 and CMV-hRad51 (K133R) were a gift from David Liu. This work was supported by National Institutes of Health (NIH) grant 1R35GM137800 to H.D. and start-up funds from the Department of Cell Biology, Microbiology and Molecular Biology (CMMB).

REFERENCES

Bétous R, Mason AC, Rambo RP, Bansbach CE, Badu-Nkansah A, Sirbu BM, Eichman BF, and Cortez D (2012). SMARCAL1 catalyzes fork regression and Holliday junction migration to maintain genome stability during DNA replication. Genes Dev. 26, 151–162. [PubMed: 22279047]

Bhat KP, Krishnamoorthy A, Dungrawala H, Garcin EB, Modesti M, and Cortez D (2018). RADX Modulates RAD51 Activity to Control Replication Fork Protection. Cell Rep. 24, 538–545. [PubMed: 30021152]

Ciccia A, Nimonkar AV, Hu Y, Hajdu I, Achar YJ, Izhar L, Petit SA, Adamson B, Yoon JC, Kowalczykowski SC, et al. (2012). Polyubiquitinated PCNA recruits the ZRANB3 translocase to maintain genomic integrity after replication stress. Mol. Cell 47, 396–409. [PubMed: 22704558]

Cimprich KA, and Cortez D (2008). ATR: an essential regulator of genome integrity. Nat. Rev. Mol. Cell Biol 9, 616–627. [PubMed: 18594563]

Cortez D (2015). Preventing replication fork collapse to maintain genome integrity. DNA Repair (Amst.) 32, 149–157. [PubMed: 25957489]

Craddock KE, Okur V, Wilson A, Gerkes EH, Ramsey K, Heeley JM, Juusola J, Vitobello A, Dupeyron MB, Faivre L, and Chung WK (2019). Clinical and genetic characterization of individuals with predicted deleterious *PHIP* variants. Cold Spring Harb. Mol. Case Stud. 5, a004200. [PubMed: 31167805]

Datta A, and Brosh RM Jr. (2019). Holding All the Cards-How Fanconi Anemia Proteins Deal with Replication Stress and Preserve Genomic Stability. Genes (Basel) 10, 170.

De Semir D, Nosrati M, Bezrookove V, Dar AA, Federman S, Bienvenu G, Venna S, Rangel J, Climent J, Meyer Tamgüney TM, et al. (2012). Pleckstrin homology domain-interacting protein (PHIP) as a marker and mediator of melanoma metastasis. Proc. Natl. Acad. Sci. USA 109, 7067–7072. [PubMed: 22511720]

Dungrawala H, Rose KL, Bhat KP, Mohni KN, Glick GG, Couch FB, and Cortez D (2015).The Replication Checkpoint Prevents Two Types of Fork Collapse without Regulating Replisome Stability. Mol. Cell 59, 998–1010. [PubMed: 26365379]

Dungrawala H, Bhat KP, Le Meur R, Chazin WJ, Ding X, Sharan SK, Wessel SR, Sathe AA, Zhao R, and Cortez D (2017). RADX Promotes Genome Stability and Modulates Chemosensitivity by Regulating RAD51 at Replication Forks. Mol. Cell 67, 374–386.e5. [PubMed: 28735897]

Farhang-Fallah J, Randhawa VK, Nimnual A, Klip A, Bar-Sagi D, and Rozakis-Adcock M (2002). The pleckstrin homology (PH) domain-interacting protein couples the insulin receptor substrate 1 PH domain to insulin signaling pathways leading to mitogenesis and GLUT4 translocation. Mol. Cell. Biol. 22, 7325–7336. [PubMed: 12242307]

Franken NA, Rodermond HM, Stap J, Haveman J, and van Bree C (2006). Clonogenic assay of cells in vitro. Nat. Protoc. 1, 2315–2319. [PubMed: 17406473]

Higgins NP, Kato K, and Strauss B (1976). A model for replication repair in mammalian cells. J. Mol. Biol 101, 417–425. [PubMed: 1255724]

Higgs MR, Reynolds JJ, Winczura A, Blackford AN, Borel V, Miller ES, Zlatanou A, Nieminuszczy J, Ryan EL, Davies NJ, et al. (2015). BOD1L Is Required to Suppress Deleterious Resection of Stressed Replication Forks. Mol. Cell 59, 462–477. [PubMed: 26166705]

Jackson DA, and Pombo A (1998). Replicon clusters are stable units of chromosome structure: evidence that nuclear organization contributes to the efficient activation and propagation of S phase in human cells. J. Cell Biol 140, 1285–1295. [PubMed: 9508763]

Jackson S, and Xiong Y (2009). CRL4s: the CUL4-RING E3 ubiquitin ligases. Trends Biochem. Sci. 34, 562–570. [PubMed: 19818632]

Jang SM, Nathans JF, Fu H, Redon CE, Jenkins LM, Thakur BL, Pongor LS, Baris AM, Gross JM, O'Neill MJ, et al. (2020). The RepID-CRL4 ubiquitin ligase complex regulates metaphase to anaphase transition via BUB3 degradation. Nat. Commun 11, 24. [PubMed: 31911655]

Jin J, Arias EE, Chen J, Harper JW, and Walter JC (2006). A family of diverse Cul4-Ddb1-interacting proteins includes Cdt2, which is required for S phase destruction of the replication factor Cdt1. Mol. Cell 23, 709–721. [PubMed: 16949367]

Kile AC, Chavez DA, Bacal J, Eldirany S, Korzhnev DM, Bezsonova I, Eichman BF, and Cimprich KA (2015). HLTF's Ancient HIRAN Domain Binds 3' DNA Ends to Drive Replication Fork Reversal. Mol. Cell 58, 1090–1100. [PubMed: 26051180]

Kolinjivadi AM, Sannino V, de Antoni A, Técher H, Baldi G, and Costanzo V (2017a). Moonlighting at replication forks - a new life for homologous recombination proteins BRCA1, BRCA2 and RAD51. FEBS Lett. 591, 1083–1100. [PubMed: 28079255]

Kolinjivadi AM, Sannino V, De Antoni A, Zadorozhny K, Kilkenny M, Técher H, Baldi G, Shen R, Ciccia A, Pellegrini L, et al. (2017b). Smarcal1-Mediated Fork Reversal Triggers Mre11-Dependent Degradation of Nascent DNA in the Absence of Brca2 and Stable Rad51 Nucleofilaments. Mol. Cell 67, 867–881.e7. [PubMed: 28757209]

Liao H, Ji F, Helleday T, and Ying S (2018). Mechanisms for stalled replication fork stabilization: new targets for synthetic lethality strategies in cancer treatments. EMBO Rep. 19, e46263. [PubMed: 30108055]

Liu L, Yin Y, Li Y, Prevedel L, Lacy EH, Ma L, and Zhou P (2012). Essential role of the CUL4B ubiquitin ligase in extra-embryonic tissue development during mouse embryogenesis. Cell Res. 22, 1258–1269. [PubMed: 22453236]

Méndez J, and Stillman B (2000). Chromatin association of human origin recognition complex, cdc6, and minichromosome maintenance proteins during the cell cycle: assembly of prereplication complexes in late mitosis. Mol. Cell. Biol 20, 8602–8612. [PubMed: 11046155]

Mijic S, Zellweger R, Chappidi N, Berti M, Jacobs K, Mutreja K, Ursich S, Ray Chaudhuri A, Nussenzweig A, Janscak P, and Lopes M (2017). Replication fork reversal triggers fork degradation in BRCA2-defective cells. Nat. Commun 8, 859. [PubMed: 29038466]

Morrison C, Shinohara A, Sonoda E, Yamaguchi-Iwai Y, Takata M, Weichselbaum RR, and Takeda S (1999). The essential functions of human Rad51 are independent of ATP hydrolysis. Mol. Cell. Biol 19, 6891–6897. [PubMed: 10490626]

Neelsen KJ, and Lopes M (2015). Replication fork reversal in eukaryotes: from dead end to dynamic response. Nat. Rev. Mol. Cell Biol 16, 207–220. [PubMed: 25714681]

Pan ZQ, Kentsis A, Dias DC, Yamoah K, and Wu K (2004). Nedd8 on cullin: building an expressway to protein destruction. Oncogene 23, 1985–1997. [PubMed: 15021886]

Pierce AJ, Johnson RD, Thompson LH, and Jasin M (1999). XRCC3 promotes homology-directed repair of DNA damage in mammalian cells. Genes Dev. 13, 2633–2638. [PubMed: 10541549]

Podcheko A, Northcott P, Bikopoulos G, Lee A, Bommareddi SR, Kushner JA, Farhang-Fallah J, and Rozakis-Adcock M (2007). Identification of a WD40 repeat-containing isoform of PHIP as a novel regulator of beta-cell growth and survival. Mol. Cell. Biol. 27, 6484–6496. [PubMed: 17636024]

Ran FA, Hsu PD, Wright J,Agarwala V, Scott DA, and Zhang F (2013). Genome engineering using the CRISPR-Cas9 system. Nat. Protoc. 8, 2281–2308. [PubMed: 24157548]

Ray Chaudhuri A, Callen E, Ding X, Gogola E, Duarte AA, Lee JE, Wong N, Lafarga V, Calvo JA, Panzarino NJ, et al. (2016). Replication fork stability confers chemoresistance in BRCA-deficient cells. Nature 535, 382–387. [PubMed: 27443740]

Rees HA, Yeh WH, and Liu DR (2019). Development of hRad51-Cas9 nickase fusions that mediate HDR without double-stranded breaks. Nat. Commun 10, 2212. [PubMed: 31101808]

Saldivar JC, Cortez D, and Cimprich KA (2017). The essential kinase ATR: ensuring faithful duplication of a challenging genome. Nat. Rev. Mol. Cell Biol 18, 622–636. [PubMed: 28811666]

Schlacher K, Christ N, Siaud N, Egashira A, Wu H, and Jasin M (2011). Double-strand break repair-independent role for BRCA2 in blocking stalled replication fork degradation by MRE11. Cell 145, 529–542. [PubMed: 21565612]

Schlacher K, Wu H, and Jasin M (2012). A distinct replication fork protection pathway connects Fanconi anemia tumor suppressors to RAD51-BRCA1/2. Cancer Cell 22, 106–116. [PubMed: 22789542]

Sidorova J (2017). A game of substrates: replication fork remodeling and its roles in genome stability and chemo-resistance. Cell Stress 1, 115–133. [PubMed: 29355244]

Sigurdsson S, Van Komen S, Petukhova G, and Sung P (2002). Homologous DNA pairing by human recombination factors Rad51 and Rad54. J. Biol. Chem. 277, 42790–42794. [PubMed: 12205100]

Taglialatela A, Alvarez S, Leuzzi G, Sannino V, Ranjha L, Huang JW, Madubata C, Anand R, Levy B, Rabadan R, et al. (2017). Restoration of Replication Fork Stability in BRCA1- and BRCA2-Deficient Cells by Inactivation of SNF2-Family Fork Remodelers. Mol. Cell 68, 414–430.e8. [PubMed: 29053959]

Wang AT, Kim T, Wagner JE, Conti BA, Lach FP, Huang AL, Molina H, Sanborn EM, Zierhut H, Cornes BK, et al. (2015). A Dominant Mutation in Human RAD51 Reveals Its Function in DNA Interstrand Crosslink Repair Independent of Homologous Recombination. Mol. Cell 59, 478–490. [PubMed: 26253028]

Webster E, Cho MT, Alexander N, Desai S, Naidu S, Bekheirnia MR, Lewis A, Retterer K, Juusola J, and Chung WK (2016). De novo *PHIP*-predicted deleterious variants are associated with developmental delay, intellectual disability, obesity, and dysmorphic features. Cold Spring Harb. Mol. Case Stud 2, a001172. [PubMed: 27900362]

Xu S, Wu X, Wu L, Castillo A, Liu J, Atkinson E, Paul A, Su D, Schlacher K, Komatsu Y, et al. (2017). Abro1 maintains genome stability and limits replication stress by protecting replication fork stability. Genes Dev. 31, 1469–1482. [PubMed: 28860160]

Zellweger R, Dalcher D, Mutreja K, Berti M, Schmid JA, Herrador R, Vindigni A, and Lopes M (2015). Rad51-mediated replication fork reversal is a global response to genotoxic treatments in human cells. J. Cell Biol 208,563–579. [PubMed: 25733714]

Zhang Y, Huang L, Fu H, Smith OK, Lin CM, Utani K, Rao M, Reinhold WC, Redon CE, Ryan M, et al. (2016). A replicator-specific binding protein essential for site-specific initiation of DNA replication in mammalian cells. Nat. Commun 7, 11748. [PubMed: 27272143]

Highlights

- DCAF14 is enriched at stalled replication forks
- DDB1, CUL4B, and DCAF14 facilitate stalled fork stability
- DCAF14 suppresses DNA2- and MRE11-mediated nascent strand degradation
- DCAF14 promotes replication fork protection in a RAD51-dependent manner

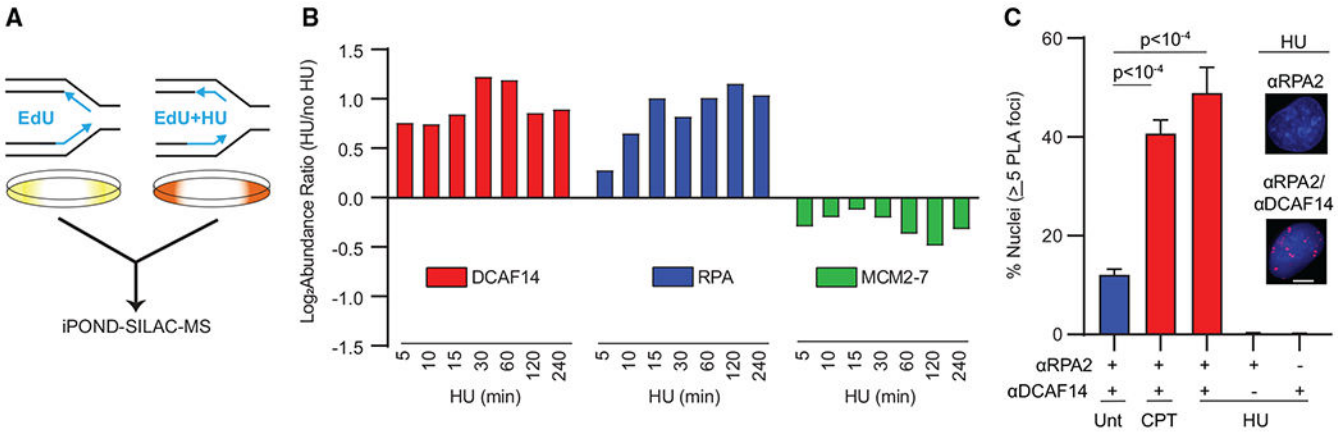

Figure 1. DCAF14 is recruited to stalled replication forks

(A) Schematic for iPOND-SILAC-mass spectrometry (MS) analyses to identify replication fork proteins in HU-treated cells.

(B) The average abundance values for selected proteins and protein complexes are shown. Complete datasets with statistics are presented elsewhere (Dungrawala et al., 2015). n = 14.

(C) *In situ* proximity ligation assay (PLA) was performed using antibodies targeting RPA32 and DCAF14. Cells were left either untreated or treated with 4 mM HU and 100 nM CPT for 4 h. Nuclei with ≥5 PLA foci were scored using 500–1,000 nuclei per sample. Mean ± SD values are representative of two biological repeats. p values were derived using one-way ANOVA. Inset: representative nuclei for HU-treated cells. Scale bar, 5 μm.

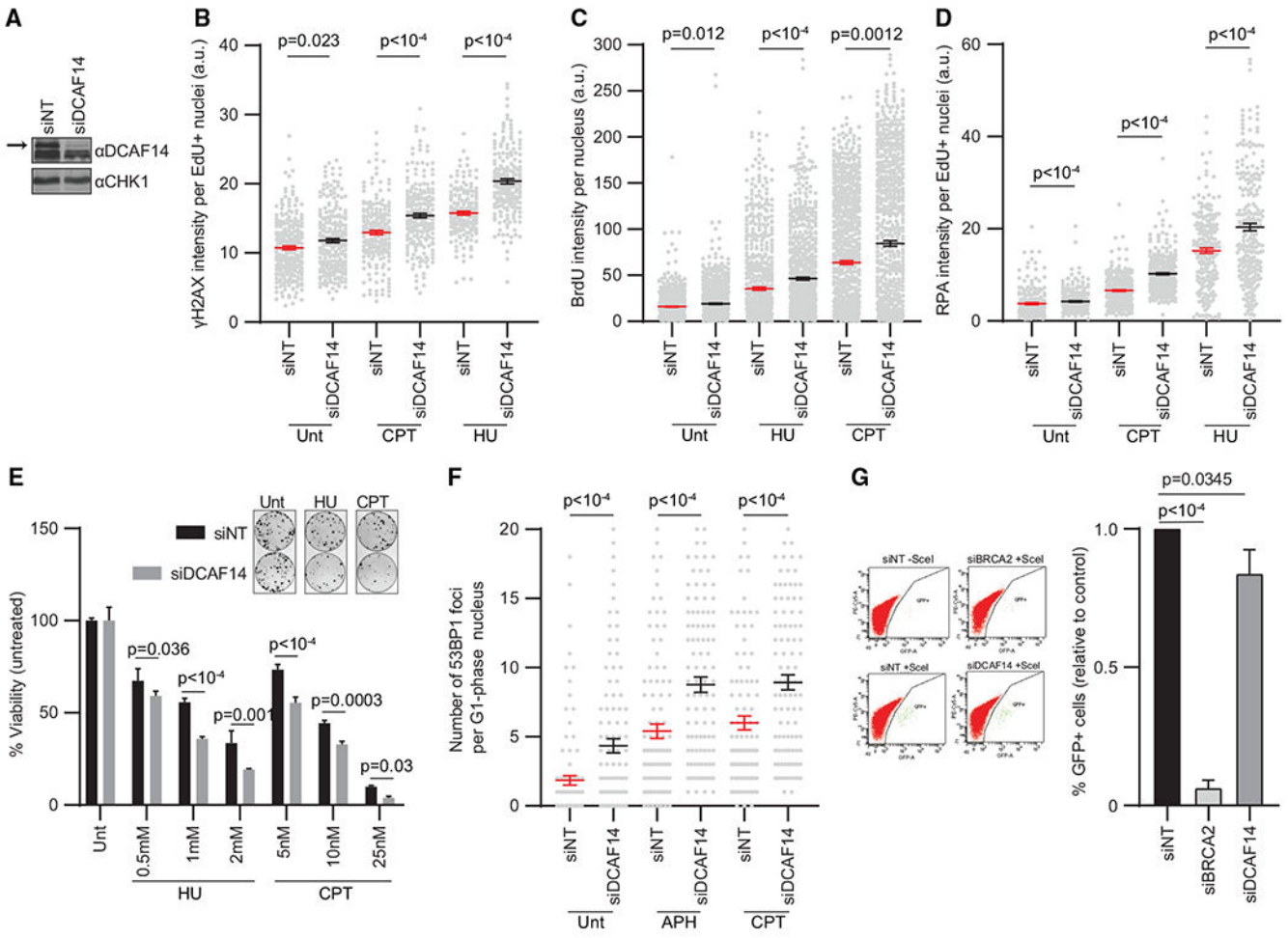

Figure 2. DCAF14 is a replication stress response protein

(A) Immunoblots of lysates harvested from U2OS cells transfected with either non-targeting siRNA (siNT)or siRNA targeting DCAF14 (siDCAF14). CHK1 serves as loading control. Arrow denotes DCAF14 protein.

(B–D) siNT- and siDCAF14-transfected U2OS cells were left either untreated or treated with 4 mM HU or 100 nM CPT for 4 h. For γH2AX and RPA staining, cells were pulsed with 5-ethynyl-2'-deoxyuridine (EdU) for 10 min prior to treatment. For native BrdU staining, cells were pulsed with 10 μM BrdU. The intensities of γH2AX and RPA were measured by quantitative imaging after preselecting EdU-positive nuclei. Mean ± SEM values are representative of three biological repeats. a.u., arbitrary units.

(E) siNT-and siDCAF14-transfected U2OS cells were plated for colony-forming assays as indicated. Inset: panel depicts representative dishes for untreated and treated conditions. All percent viability calculations were derived relative to untreated cells (mean ± SD, n = 3).

(F) siRNA-transfected U2OS cells were left untreated or treated with 0.2 μM aphidicolin (APH) or 100 nM CPT for 24 h. 53BP1 foci were measured in nuclei without detectable proliferating cell nuclear antigen (PCNA) staining. Mean ± SEM values are representative of three biological repeats.

(G) DR-GFP U2OS reporter cells were transfected with indicated siRNAs and analyzed by flow cytometry following transfection with I-Scel expression vector. Percent GFP values were normalized to control (siNT), and values were plotted using three replicates (mean ± SD). For (B)–(D) and (F), p values were derived using Mann-Whitney tests. For(E) and (G), p values were derived using multiple t test and unpaired t test, respectively. At least 150 nuclei were analyzed for(B)–(D), and 100 nuclei were analyzed for (F).
See also Figure S1.

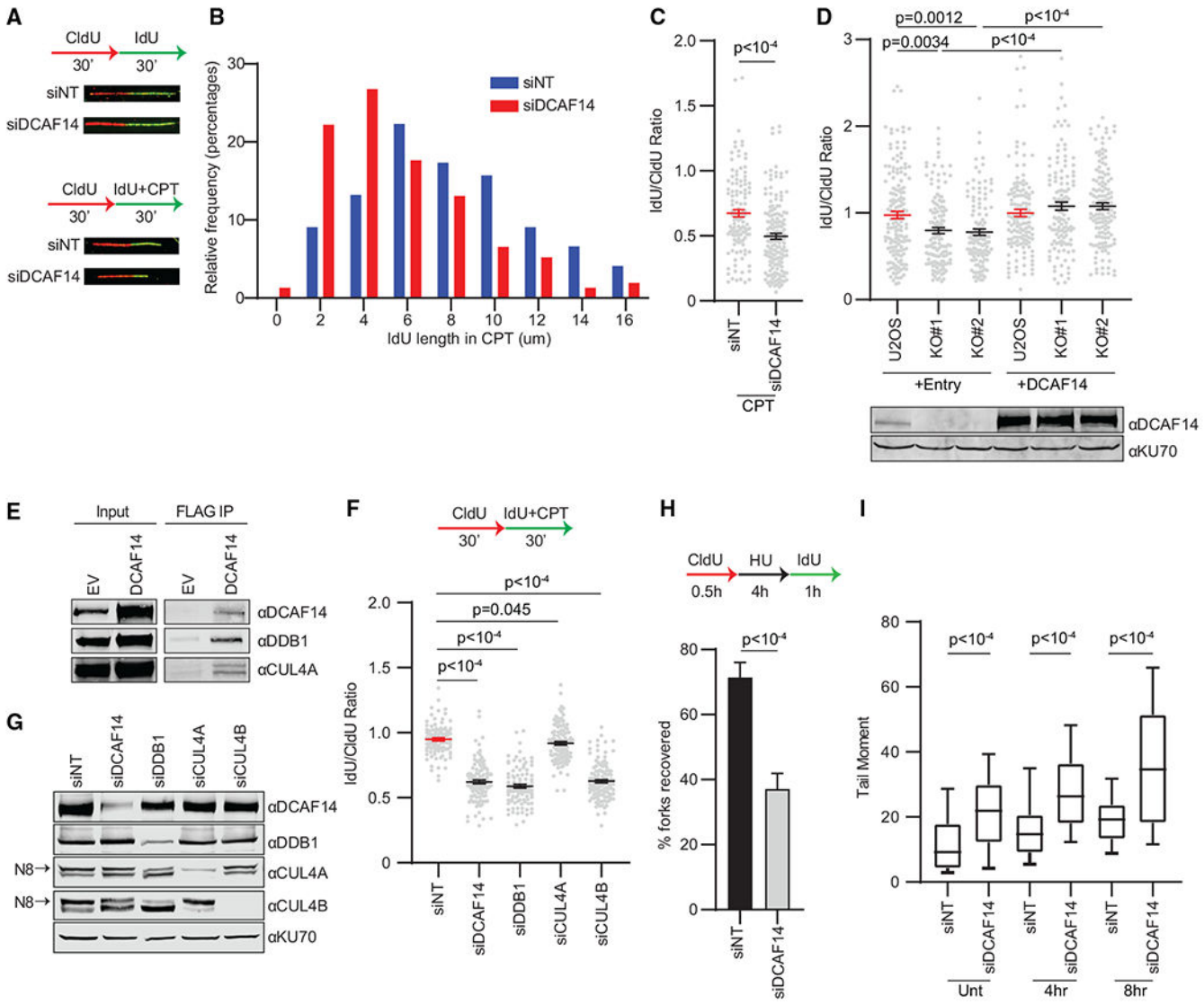

Figure 3. Loss of DCAF14 impairs fork stability and fork recovery

(A) Schematic for DNA fiber assays. Representative fiber images for indicated samples are shown.

(B and C) siNT and siDCAF14-transfected U2OS cells were pulsed using labeling scheme in presence of CPT. CldU and IdU lengths were measured, and lengths were plotted as histograms in (B) and as ratios in (C).

(D) Parental U2OS cells or DCAF14 KO clones transfected with entry vector or DCAF14 cDNA were pulsed using labeling scheme in presence of CPT, and IdU/CldU ratios were plotted. Immunoblot depicts DCAF14 expression levels and KU70 represents loading control.

(E) Whole-cell lysates for the indicated samples were immunoprecipitated using FLAG resin, and immunoprecipitates were probed with the indicated antibodies. Representative blot is shown from three biological repeats.

(F) U2OS cells transfected with the indicated siRNAs were pulsed with CldU for 30 min followed by IdU with 100 nM CPT for 30 min, and IdU/CldU ratios were plotted.
(G) Representative immunoblot depicting knockdown efficiencies for the indicated siRNAs is shown from two biological repeats. KU70 serves as loading control. Arrow represents neddylated species.
(H) siNT- and siDCAF14-transfected U2OS cells were treated as shown. Fibers with both CldU and IdU labels were scored as a percentage of all fibers imaged.
(I) Comet tails were measured for indicated cells with or without HU using neutral comet assay. Box-and-whiskers plots depicting 10–90 percentile are plotted using at least 100 nuclei. At least 120 fibers were analyzed, and representative mean ± SEM values from two biological replicates are plotted in (C), (D), (F), and (H). p values were derived using Mann-Whitney tests in (C), (D), (F), and (I). Unpaired t test was used in (H).
See also Figure S2.

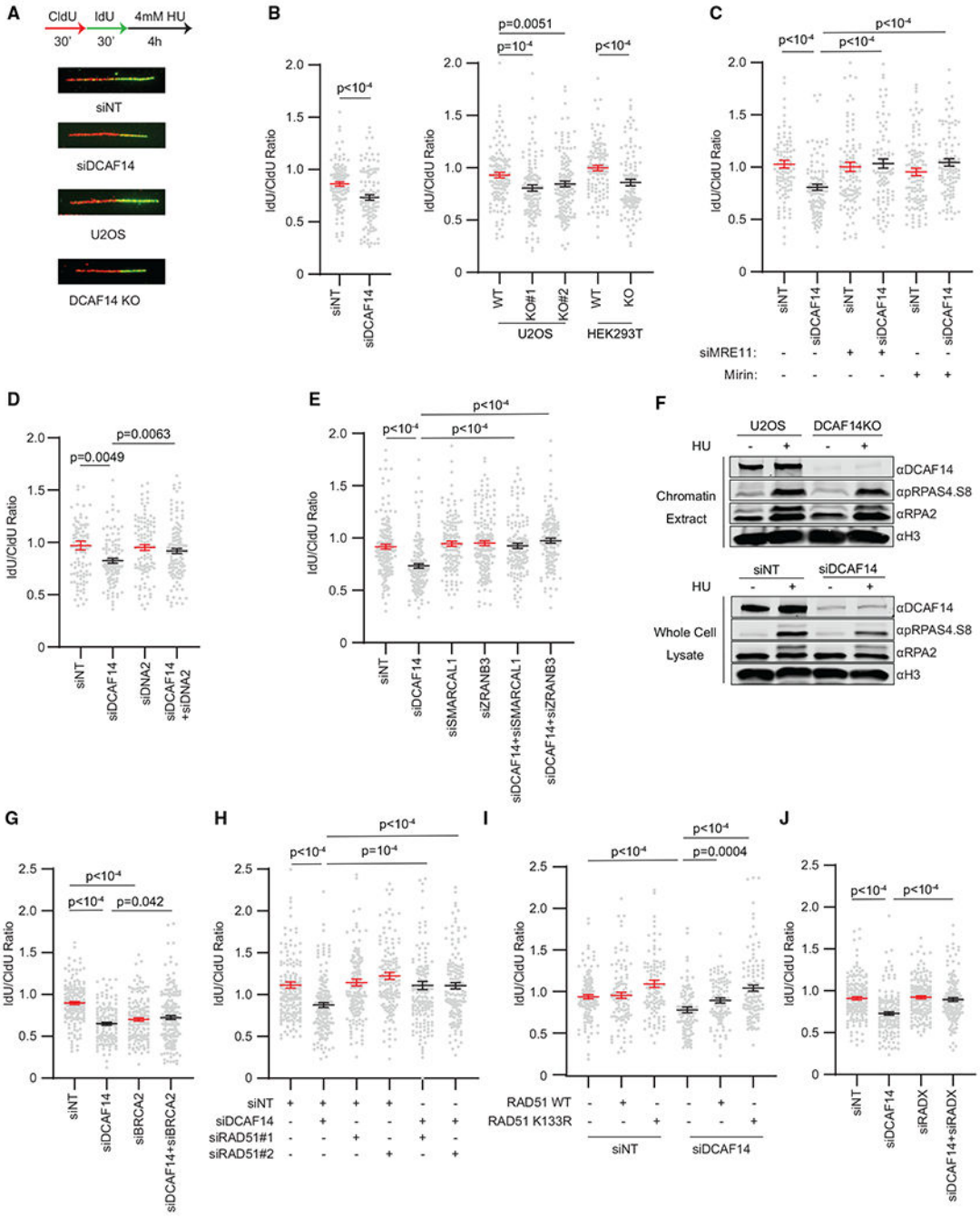

Figure 4. DCAF14 mediates replication fork protection

(A) Schematic for fork degradation assays is depicted. Representative fiber images for indicated samples are shown.

(B–E and G–J) Fork degradation assays were performed in U2OS cells using the indicated siRNAs. In (C), MRE11 inhibitor Mirin was used as indicated. In (I), cells were transfected with constructs expressing either wild-type RAD51 or K133R mutant RAD51. IdU/CldU ratios for individual experiments are plotted. Mean ± SEM values are representative of at

least two biological repeats. At least 120 fibers were analyzed. p values were derived using Mann-Whitney tests.

(F) Parental U2OS and DCAF14 KO cells (top) and siNT- and siDCAF14-transfected U2OS cells (bottom) were either left untreated or treated with 4 mM HU for 4 h. Chromatin extracts and whole-cell lysates were isolated as shown, separated using SDS-PAGE, and probed for the indicated antibodies by immunoblotting.

See also Figures S3 and S4.

KEY RESOURCES TABLE

REAGENT or RESOURCE	SOURCE	IDENTIFIER
Antibodies		
Anti-phospho-histone H2AX clone JBW301	Millipore	Cat#05-636; RRID:AB_2755003
Rabbit polyclonal anti-53BP1	Abcam	Cat#21083; RRID:AB_722496
Mouse monoclonal anti-PCNA	Santa Cruz Biotechnology	Cat#sc-56; RRID:AB_628110
Mouse monoclonal anti-CHK1	Santa Cruz Biotechnology	Cat#sc-8408; RRID:AB_627257
Mouse monoclonal anti-SMARCAL1	Santa Cruz Biotechnology	Cat#sc376377; RRID:AB_10987841
Rabbit polyclonal anti-ZRANB3	Bethyl Labs	Cat#A303-033A; RRID:AB_10773114
Mouse monoclonal anti-BRCA2	Millipore Sigma	Cat#OP95; RRID:AB_2067762
Mouse monoclonal anti-BRCA1	Santa Cruz Biotechnology	Cat#sc6954; RRID:AB_626761
Mouse monoclonal anti-BLM	Santa Cruz Biotechnology	Cat#sc365753; RRID: AB_10851630
Rabbit monoclonal anti-KU70	Abcam	Cat#ab92450; RRID:AB_10562280
Rabbit polyclonal anti-RAD51	Abcam	Cat#ab63801; RRID:AB_1142428
Rabbit polyclonal anti-H3	Abcam	Cat#ab1791; RRID:AB_302613
Mouse monoclonal anti-RPA32	Abcam	Cat#ab2175; RRID:AB_302873
Rabbit polyclonal anti-phospho RPA32 (S4/S8)	Bethyl Labs	Cat#A300-245A; RRID:AB_210547
Rabbit polyclonal anti-PHIP	Abcam	Cat#ab86244; RRID:AB_1925318
Rabbit polyclonal anti-PHIP	Novus Biologicals	Cat#NBP2-33883
Rabbit polyclonal anti-RADX	Novus Biologicals	Cat#NBP2-13887; RRID:AB_2687552
Rabbit polyclonal anti-MRE11	Cell Signaling Technology	Cat#4895S; RRID:AB_2145100
Rabbit polyclonal anti-DNA2	Invitrogen	Cat#PA5-77943; RRID:AB_2735727
Rabbit polyclonal anti-CUL4A	Abcam	Cat#ab72548; RRID:AB_1268363
Mouse monoclonal anti-CUL4B	Bio-rad	Cat#VMA00360
Rabbit polyclonal anti-DDB1	Cell Signaling Technology	Cat#5428S; RRID:AB_10634753
Mouse anti-BrdU	BD Biosciences	Cat#347580; RRID:AB_10015219
Rat monoclonal anti-BrdU	Abcam	Cat#ab6326; RRID:AB_305426
Alexa Fluor 488 Azide	Invitrogen	Cat#A10266
Alexa Fluor 594 Azide	Invitrogen	Ca#A10270
Bacterial and virus strains		
DH5α	Invitrogen	Cat#18265017
Chemicals, peptides, and recombinant proteins		
ProLong Gold Antifade Mountant	Invitrogen	Cat#P36930
ProLong Gold Antifade Mountant with DAPI	Invitrogen	Cat#P36931
FuGENE® HD Transfection Reagent	Promega	Cat#E2311
DharmaFECT 1 Transfection Reagent	Dharmacon	Cat#T-2001-03
Puromycin Dihydrochloride	GIBCO	Cat#A1113803
CldU	Millipore Sigma	Cat#C6891
IdU	Millipore Sigma	Cat#I7125

REAGENT or RESOURCE	SOURCE	IDENTIFIER
EdU	Cayman Chemical Company	Cat#20518
Propidium Iodide	Invitrogen	Cat#00-6990-50
Polyethylenimine	Polysciences Inc	Cat#23966
Hydroxyurea	Millipore Sigma	Cat#H8627
Camptothecin	Selleckchem	Cat#S1288
Aphidicolin	Millipore Sigma	Cat#178273
Cisplatin	USP	Cat# 1134357
Olaparib	Selleckchem	Cat# S1060
Critical commercial assays		
Duolink *In Situ* Red Starter Kit Mouse/Rabbit	Millipore Sigma	Cat#DUO92101
Comet assay kit	Trevigen	Cat#4250-050-ESK
Deposited Data		
Raw data	This paper	http://dx.doi.org/10.17632/2785zxsyzd.1
Experimental models: cell lines		
U2OS	ATCC	Cat#HTB-96; RRID:CVCL_0042
HEK293T	ATCC	Cat#CRL-3216; RRID:CVCL_0063
RPE-hTERT	ATCC	Cat#CRL-4000; RRID:CVCL_4388
DR-GFP U2OS	Pierce et al., 1999	N/A
Oligonucleotides		
DCAF14 siRNA	Dharmacon	Cat#J-019291-05
DCAF14 siRNA	Dharmacon	Cat#J-019291-06
DCAF14 siRNA	Dharmacon	Cat#J-019291-07
DCAF14 siRNA	Dharmacon	Cat#J-019291-08
DDB1 siRNA	Dharmacon	Cat#L-012890
RADX siRNA	Dharmacon	Cat#J-014634
RAD51 siRNA	Dharmacon	Cat#J-003530-11
RAD51 siRNA	Dharmacon	Cat#J-003530-12
MRE11 siRNA	Dharmacon	Cat#J-009271-08
SMARCAL1 siRNA	Dharmacon	Cat#J-013058-06
CUL4A siRNA	Dharmacon	Cat#L-012610
CUL4B siRNA	Dharmacon	Cat#L-017965
DNA2 siRNA	Dharmacon	Cat#D-026431-03
DNA2 siRNA	Dharmacon	Cat#D-026431-04
ZRANB3 siRNA	Dharmacon	Cat#D-010025-03
BRCA1 siRNA	Dharmacon	Cat#J-003461
BLM siRNA	Dharmacon	Cat#L-007287
BRCA2 siRNA	QIAGEN	Cat#SI02653434
All-stars negative control siRNA	QIAGEN	Cat#1027280
Recombinant DNA		

REAGENT or RESOURCE	SOURCE	IDENTIFIER
pSpCas9(BB)-2A-Puro (PX459) V2.0	Ran et al., 2013	Addgene Cat#62988
pCMV6-Entry Mammalian Expression Vector	Origene	Cat#PS100001
PHIP (NM_017934) Human Tagged ORF Clone	Origene	Cat#RC217114
CMV-hRad51	Rees et al., 2019	Addgene Cat#125570
CMV-hRad51(K133R)	Rees et al., 2019	Addgene Cat#125571
Software and algorithms		
Graphpad Prism	Graphpad software	https://www.graphpad.com/scientific-software/prism/
ImageJ	NIH	https://imagej.nih.gov/ij/download.html
Cell Profiler	Broad Institute	https://cellprofiler.org/
Comet Score	Tritek	http://www.cometassay.com/index_files/Page484.htm